Use of Fano resonances for bistable optical transfer through photonic crystal films

Virginie Lousse[1,2,*] and Jean Pol Vigneron[1]
[1]*Laboratoire de Physique du Solide, Facultés Universitaires Notre-Dame de la Paix, 61 rue de Bruxelles, B-5000 Namur, Belgium*
[2]*Department of Electrical Engineering, Stanford University, Stanford, California 94305, USA*
(Received 26 November 2003; revised manuscript received 2 February 2004; published 14 April 2004)

Bistable or multistable transmissions are classically the result of the introduction of nonlinear layers into a resonant Fabry-Perot cavity. A single inhomogeneous film, with a periodic lateral structure, can also give rise to a bistable transmission for significant intensity ranges, due to Fano resonances, a strong frequency-dependent transparency variation related to the transfer via guided modes. A self-consistent simulation tool which allows for the computation of multivalued transmission is developed and the peculiar shape of the hysteresis loops associated with Fano resonances is studied.

DOI: 10.1103/PhysRevB.69.155106 PACS number(s): 78.67.Pt, 78.66.−w, 42.70.Qs

I. INTRODUCTION

Optical bistability generally occurs at carefully chosen frequencies, when a nonlinear Fabry-Perot-type resonant cavity transmits high intensity light.[1] The initial ingredient needed to produce a multivalued transparency is a sharp peak in the spectral transmission, so that it is commonly believed that the design of a bistable filter should start with the installation of two reflectors, creating a high-finesse resonant cavity. This ''Lorentzian'' bistable device, governed by the careful alignment of two reflecting films, has received much attention, and the hysteresis cycle which develops in these nonlinear structures has been described, both theoretically and experimentally.[2–4]

The nonlinear behavior of inhomogeneous structures and, in particular, periodic ones has been investigated by several authors.[5–7] Fabry-Perot resonators and ''Kerr'' materials are the basic ingredients of several cleverly engineered structures, all expected to open the road to the optical control of optical signals.[8] The optical transistor[9] transfers a signal modulation from a first to a second light beam. An optical discriminator[10] is transparent to a light pulse only when its amplitude exceeds a fixed threshold. An optical limitor[11] saturates its output intensity so that it becomes independent of the incident intensity for strong signals. A pulse shaper can be designed, for instance, with a Fabry-Perot interferometer tuned for transparency for a specific pulse wave packet, and detuned by the presence of the pulse itself.[12] An optical trigger[13] delivers a strong light pulse upon reception of a command optical signal. An optical oscillator[11] produces a beating signal from a stationary, constant amplitude beam of light. All these signal-processing tools require a nonlinear behavior of the material which completely or partially fills the resonator cavity.

Logical gates can also be developed from a nonlinear resonator,[14] and the optical memory switching between two[9] or several stable states[15] has been demonstrated.

In the present work, we wish to emphasize the use of new spectral features, found in single photonic-crystal films, to possibly produce bistability. These spectral features are usually referred to as ''Fano'' resonances[16] and have been shown to dominate the reflection or transmission spectra of corrugated dielectric films.[17]

The paper is organized as follows. First, we introduce the extension of the transfer-matrix technique required to describe nonlinear, multivalued transmissions. Then, after briefly discussing the origin of the asymmetric Fano transmission profiles in the linear-response regime, we will describe the mechanisms of bistability based on the spectral displacement of Fano line shapes with the transiting intensity, due to the nonlinear response.

II. SELF-CONSISTENT TRANSMISSION COEFFICIENTS OF A PHOTONIC-CRYSTAL FILM

We first briefly sketch the self-consistent procedure which allows to determine the intensity-dependent and possibly multivalued transmission through a nonlinear, three-dimensional, photonic-crystal film. The computing strategy is designed to reduce the nonlinear approach to a converging sequence of simpler, linear computations. Similar ideas[18] were used for the calculation of *infinite* nonlinear photonic-crystal band structures,[19] where the technique is reminiscent of the self-consistent treatment of many-particle ground state in quantum mechanics.[20]

We consider a film of three-dimensional photonic crystal containing nonlinear materials. The type of nonlinearity considered here is restricted to the ''optical Kerr effect,'' where the volume refractive index of the material is modified linearly with the square of the local electric field:

$$n(\vec{r}) = n_0(\vec{r}) + n_2(\vec{r})|\vec{E}(\vec{r})|^2. \quad (1)$$

Reading this expression, $n_0(\vec{r})$ is the refractive index in the absence of transiting light, $n(\vec{r})$ is the refractive index modified by the illumination, and $\vec{E}(\vec{r})$ is the local electric field. The nonlinear refraction coefficient of the Kerr material at the location $\vec{r}$, expressed in units of $m^2\,V^{-2}$, is denoted by $n_2(\vec{r})$.

The nonlinear transmission is a self-consistent process: the cavity transparency controls the transmitted wave which, in turn, controls the value of the Kerr medium refractive index. This, by acting on the optical path, reacts back on the transparency.

The transmission coefficient of the film, summed over all transmitted beams, is a functional of the inhomogeneous refractive index:

$$\mathcal{T}=\mathcal{T}[n(\vec{r})], \tag{2}$$

and, in the present work, we use a transfer-matrix technique[21] to proceed with its construction. Moreover, the square of the electric field is a nonlocal functional of the index distribution, while it depends on the square modulus of the incident field $\vec{E}_0$,

$$|\vec{E}(\vec{r})|^2=\mathcal{E}[n(\vec{r}),|\vec{E}_0|^2]. \tag{3}$$

The building scheme of this functional being assumed to be known, the nonlinear transmission is virtually obtained, as the square modulus of the electric field can be extracted from the following nonlinear equation:

$$|\vec{E}(\vec{r})|^2=\mathcal{E}[n_0(\vec{r})+n_2(\vec{r})|\vec{E}(\vec{r})|^2,|\vec{E}_0|^2]. \tag{4}$$

This relation requires that the square of the modulus of the electric field should be brought to self-consistency: introduced in the right-hand side expression, this quantity should behave as a ''fixed scalar field'' for Eq. (4). From a more technical point of view, an iterative approach can be applied, starting with a reasonable approximation of the refractive index and its associated squared electric field, introducing it in the right-hand side of Eq. (4) to attempt to refine it, repeating this refinement step iteratively, until adequate convergence is reached. In case of slow, or even lack of convergence of this process, acceleration schemes are known, which extrapolate the new field from several past iterates. For instance, the corrector step

$$|\vec{E}(\vec{r})|^2_{out}=\alpha|\vec{E}(\vec{r})|^2_{out}+(1-\alpha)|\vec{E}(\vec{r})|^2_{in} \tag{5}$$

with an appropriate value of α has been found adequate in our simulations.

The initial field used to start the iterations could be the field obtained with the unmodified refractive index $n_0(\vec{r})$. However, this procedure would not allow to describe bistable transmission, as the convergence would always occur onto the same field state. This is not advisable, as several solutions of Eq. (4) may exist for the same value of the source parameters, i.e., the same incident intensity. Some of these states are stable (a slight change of the incident intensity leads only to a slight modification of the transmission); some others are unstable (a small change of the incident intensity causes a drastic modification of the transmission). Under convergence, the iterative process can only lead—by definition—to stable states. This allows to handle bistability situations in a quite elegant way: starting with a very low intensity, the transmission coefficient is iterated, taking, as a starting refractive index, the ''dark'' limit $n_0(\vec{r})$. This converges to a new, corrected refractive index $n(\vec{r})$, which is used as a starting point for the next, increased intensity. The converged transmissions then follow the branch of stable states varying continuously from the low-intensity limit, until this state eventually ceases to exist in a bistable hysteresis loop. Then, as will be shown in examples below, for even higher intensities, the system is forced to converge to another transparency state and suddenly jumps to a very different transmission coefficient. This new state is maintained as the only stable convergence limit when the incident intensity is further increased, but also, when bistability occurs, when the intensity is decreased to already explored values. The hysteresis loops can then be described if the various incident intensities are explored in slowly increasing or decreasing sequences and if the self-consistent iterations are carried out in such a way that the starting refractive index of the iterations for a new incident intensity is the final, converged value found in the previous, slightly different, incident intensity. For most incident intensities, the number of iterations is very reasonable (10 is a typical number), except at the switching thresholds, where a few hundreds iteration steps are often required.

III. EVALUATION OF THE ELECTRIC FIELD AND TRANSMISSION FUNCTIONALS

We now turn to a brief account of the evaluation of the functionals in Eqs. (2) and (3), in the case of a photonic-crystal film with a given distribution $n(\vec{r})$ of the refractive index.

The transmission coefficient functional $\mathcal{T}$ is computed in the framework of the transfer-matrix formalism, by first splitting the film into a finite number N of thin layers, creating $N+1$ interfaces, located at the abscissas z_p, $p=0,1,2,\ldots,N$. On each of these interfaces (a region of zero length), where the refractive index is assumed to be that of the incidence region $\sqrt{\varepsilon}$, the fields are given the form of plane waves,

$$\begin{aligned}\vec{E}(\vec{\rho},z_p)=&\sum_{\vec{g}} N^{+}_{p\vec{g}}\vec{\eta}_{\vec{g}}e^{ik_{\vec{g}z}(z-z_p)}e^{i(\vec{k}_{//}+\vec{g})\vec{\rho}}\\&+\sum_{\vec{g}} N^{-}_{p\vec{g}}\vec{\eta}_{\vec{g}}e^{-ik_{\vec{g}z}(z-z_p)}e^{i(\vec{k}_{//}+\vec{g})\vec{\rho}}\\&+\sum_{\vec{g}} X^{+}_{p\vec{g}}\vec{\chi}^{+}_{\vec{g}}e^{ik_{\vec{g}z}(z-z_p)}e^{i(\vec{k}_{//}+\vec{g})\vec{\rho}}\\&+\sum_{\vec{g}} X^{-}_{p\vec{g}}\vec{\chi}^{-}_{\vec{g}}e^{-ik_{\vec{g}z}(z-z_p)}e^{i(\vec{k}_{//}+\vec{g})\vec{\rho}}\end{aligned} \tag{6}$$

for the electric field, and

$$\begin{aligned}\vec{H}(\vec{\rho},z_p)=&-\frac{\sqrt{\varepsilon}}{c\mu_0}\sum_{\vec{g}} N^{+}_{p\vec{g}}\vec{\chi}^{+}_{\vec{g}}e^{ik_{\vec{g}z}(z-z_p)}e^{i(\vec{k}_{//}+\vec{g})\vec{\rho}}\\&-\frac{\sqrt{\varepsilon}}{c\mu_0}\sum_{\vec{g}} N^{-}_{p\vec{g}}\vec{\chi}^{-}_{\vec{g}}e^{-ik_{\vec{g}z}(z-z_p)}e^{i(\vec{k}_{//}+\vec{g})\vec{\rho}}\\&+\frac{\sqrt{\varepsilon}}{c\mu_0}\sum_{\vec{g}} X^{+}_{p\vec{g}}\vec{\eta}_{\vec{g}}e^{ik_{\vec{g}z}(z-z_p)}e^{i(\vec{k}_{//}+\vec{g})\vec{\rho}}\\&+\frac{\sqrt{\varepsilon}}{c\mu_0}\sum_{\vec{g}} X^{-}_{p\vec{g}}\vec{\eta}_{\vec{g}}e^{-ik_{\vec{g}z}(z-z_p)}e^{i(\vec{k}_{//}+\vec{g})\vec{\rho}}\end{aligned} \tag{7}$$

for the magnetic field. Only the continuous components parallel to the film surface need to be known. In these expressions the summation covers the reciprocal-lattice vectors $\vec{g}$ associated with the two-dimensional periodicity parallel to the photonic-crystal film. The Bloch wave vector $\vec{k}_{//}$ is selected in the two-dimensional Brillouin zone when defining the incident wave, and, for a harmonic wave with angular frequency ω, the local normal wave vector is

$$k_{\vec{g}z} = \sqrt{\varepsilon \frac{\omega^2}{c^2} - |\vec{k}_{//} + \vec{g}|^2}. \tag{8}$$

The polarization vectors can be written as

$$\vec{\eta}_{\vec{g}} = \frac{(\vec{k}_{//} + \vec{g})}{|\vec{k}_{//} + \vec{g}|} \times \vec{e}_z, \tag{9}$$

and

$$\vec{\chi}_{\vec{g}}^{\pm} = \mp \frac{k_{\vec{g}z} c}{\omega \sqrt{\varepsilon}} \frac{\vec{k}_{//} + \vec{g}}{|\vec{k}_{//} + \vec{g}|} + \frac{|\vec{k}_{//} + \vec{g}| c}{\omega \sqrt{\varepsilon}} \vec{e}_z. \tag{10}$$

Maxwell's equations allow to produce the scattering matrix S_p, which relates the outgoing waves (r^- with coefficients N_p^- and X_p^-, and t^+ with coefficients N_{p+1}^+ and X_{p+1}^+) to the ingoing waves (i^+ with coefficients N_p^+ and X_p^+, and i^- with coefficients N_{p+1}^- and X_{p+1}^-) for each layer,

$$\begin{bmatrix} t^+ \\ r^- \end{bmatrix} = \begin{bmatrix} S^{++} & S^{+-} \\ S^{-+} & S^{--} \end{bmatrix} \begin{bmatrix} i^+ \\ i^- \end{bmatrix}. \tag{11}$$

For multilayer films, these scattering matrices are assembled[21] using the following stable expressions [Eq. (12)]. If a layer which scatters the light with the scattering matrix S_2 is added on the emergence side of a layer which scatters the light with the scattering matrix S_1, the global scattering matrix S is constructed as

$$\begin{aligned} S^{++} &= S_2^{++}(1 - S_1^{+-} S_2^{-+})^{-1} S_1^{++}, \\ S^{+-} &= S_2^{+-} + S_2^{++}(1 - S_1^{+-} S_2^{-+})^{-1} S_1^{+-} S_2^{--}, \\ S^{-+} &= S_1^{-+} + S_1^{--} S_2^{-+}(1 - S_1^{+-} S_2^{-+})^{-1} S_1^{++}, \\ S^{--} &= S_1^{--}[1 + S_2^{-+}(1 - S_1^{+-} S_2^{-+})^{-1} S_1^{+-}] S_2^{--}. \end{aligned} \tag{12}$$

The scattering matrix which represents the wave admission from the incidence region, and the one which expresses the exit to the emergence region should not be left out of the global film S matrix. Once this photonic-crystal film S matrix is known for the given refractive index $n(\vec{r})$, the value of the transmission functional $\mathcal{T}[n(\vec{r})]$ is found as the ratio of the transmitted current,

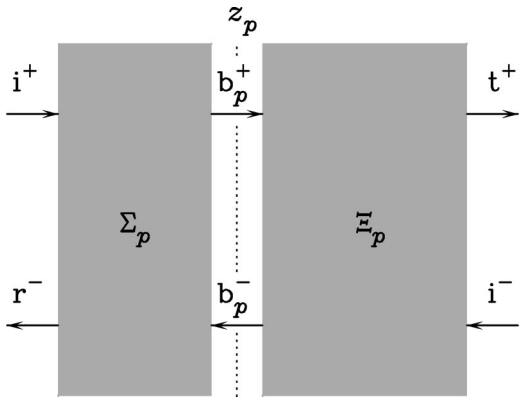

FIG. 1. Geometry for the calculation of the square modulus of the electric field of a photonic-crystal film as a functional of the inhomogeneous refractive index. The field components parallel to the film are computed at the boundary between two joining layers of the film. This requires the evaluation of two partial scattering matrices Σ_p and Ξ_p.

$$J(t^+) = \frac{\sigma_{cell}}{2\mu_0 \omega} \sum_{\vec{g}} k_{N+1\vec{g}z} [|N_{N+1\vec{g}}^+|^2 + |X_{N+1\vec{g}}^+|^2] \Theta\left(\varepsilon_{N+1} \frac{\omega^2}{c^2} - |\vec{k}_{//} + \vec{g}|^2 \right), \tag{13}$$

to the incident current

$$J(i^+) = \frac{\sigma_{cell} \sqrt{\varepsilon} \cos\theta}{2\mu_0 c} [|\sigma_{\vec{g}=0}^s|^2 + |\sigma_{\vec{g}=0}^p|^2] \tag{14}$$

carried by a single incident wave, with incidence angle θ and a mixing of s (TE) and p (TM) polarizations with respective amplitudes $\sigma_{\vec{g}=0}^s$ and $\sigma_{\vec{g}=0}^p$.

The functional which defines the square of the electric field throughout the structure is easily evaluated in the framework of the above transfer-matrix formalism. The idea is to compute the (x,y) components of the electric and magnetic fields on all layer boundaries from the plane-wave coefficients N_p^+, X_p^+, N_p^-, and X_p^-, and interpolate these continuous field components inside each layer. Then Ampere law, in Maxwell's equations, allows to make the electric field information complete, by providing the explicit value of the discontinuous z component of the field. For very thin layers, the square modulus of the electric field may be considered independent of the depth z in the layer. For a given interface, at $z = z_p$, the calculation of the field coefficients requires two partial scattering matrices (see Fig. 1): the first one (Σ) represents the scattering by all the layers of the film between the interface and the incidence region, and the second one (Ξ) represents the scattering by all the layers of the film between the interface and the emergence region. Denoting by b_p^+ and b_p^- the coefficients of the waves (respectively, from incidence to emergence, and from emergence to incidence regions) on interface z_p, we have

$$\begin{bmatrix} b_p^+ \\ r^- \end{bmatrix} = \begin{bmatrix} \Sigma_p^{++} & \Sigma_p^{+-} \\ \Sigma_p^{-+} & \Sigma_p^{--} \end{bmatrix} \begin{bmatrix} i^+ \\ b_p^- \end{bmatrix} \tag{15}$$

and

$$\begin{bmatrix} t^+ \\ b_p^- \end{bmatrix} = \begin{bmatrix} \Xi_p^{++} & \Xi_p^{+-} \\ \Xi_p^{-+} & \Xi_p^{--} \end{bmatrix} \begin{bmatrix} b_p^+ \\ i^- \end{bmatrix}. \tag{16}$$

In these expressions, r^-, i^+, t^+, and i^- contain the wave amplitudes in the incidence and emergence regions, as determined by the full-film scattering matrix and the incident wave. The requested interface coefficients are then easily obtained:

$$b_p^+ = (1 - \Sigma_p^{+-} \Xi_p^{-+})^{-1} \Sigma_p^{++} i^+ \tag{17}$$

and

$$b_p^- = \Xi_p^{-+} b_p^+ . \tag{18}$$

These considerations actually extend the widely used electromagnetic transfer-matrix technique to make it suitable for handling nonlinear layers and provide its incident-intensity-dependent transmission coefficient. As will be seen in the remaining part of this paper, the same extension is also instrumental in providing detailed information on the bistable behavior of inhomogeneous dielectric films.

IV. FANO ASYMMETRIC TRANSMISSION PROFILES

The lateral corrugation of a bidimensional periodic film has a very significant impact on the transmission spectrum (from now on, ''lateral'' means parallel to the film surfaces). In a homogeneous film, standing waves lead to symmetric, Lorentzian structures. If the film exhibits a periodic variation of the refractive index in the lateral directions, new spectral structures show up due to the possible hybridization of guided and radiative modes. These structures are recognizable, as they produce characteristic asymmetric profiles in the transmission or reflection spectra. These asymmetric lines indicate Fano resonances,[16] described as typical feature of periodically corrugated films.[17]

Figure 2 shows the photonic structure of a thin dielectric film, with a thickness d and a nondispersive dielectric constant ε. With a flat, homogeneous film, two classes of ''modes'' can be distinguished. The first comprises the guided modes, characterized by an evanescent behavior of the outer field and sharp dispersion relations below the light line $\omega = k_y c$. These dispersion relations are asymptotic to a new light line $\omega = k_y c/\sqrt{\varepsilon}$ which describes the wave propagation in an infinite medium of dielectric constant equal to that of the film (ε). For a given value of the parallel wave vector k_y, a finite number of guided modes is found, which corresponds to the installation of standing waves in the thickness of the film. These standing waves essentially differ by the normal component k_z of the wave vector ($k_z^2 c^2 = \varepsilon \omega^2 - k_y^2 c^2$). This component controls the internal incidence angle so that higher frequencies lead to more normal incidence, until the total internal reflection angle is passed over and the modes become radiative.

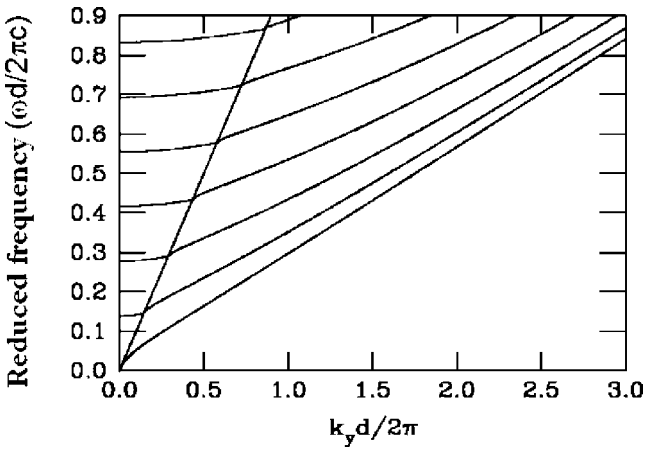

FIG. 2. Dispersion relations of the modes TE of a flat, homogeneous film of constant thickness d, in vacuum. Here, the dielectric constant of the film is chosen to be $\varepsilon = 13$. One distinguishes the guided modes, under the vacuum light line $\omega = k_y c$, and the diffused, radiative modes above the vacuum light line.

In the frequency domain above the vacuum light line, there is no guided mode, as the waves outside the film recover a real wave vector, and are able to carry an electromagnetic current and draw energy from the slab. The transmission is maximum for resonance frequencies ω_m which closely verify

$$\frac{\omega_m d}{2\pi c} = m \frac{1}{2\sqrt{\varepsilon}} \tag{19}$$

for $k_y \approx 0$. These resonances all have the same lifetime which leads to a Lorentzian profile with a half-width Γ_0 that can be expressed by

$$\frac{\Gamma_0 d}{2\pi c} = \frac{1}{\pi(1+\varepsilon)}. \tag{20}$$

This turns out to be rather large, even for films made from a very high refractive index material. For $\varepsilon = 13$, for instance, the line width turns out, in reduced units, to be 0.023, which represents a significant fraction of the distance, in reduced frequency, between successive resonances.

The two types of modes we have just described—guided and radiative—are strictly independent in a flat, infinite homogeneous film. They appear in different regions of the plane (ω, k_y) and cannot exchange energy or decay into each other. The situation changes when refractive index inhomogeneities appear in the film. The above guided and radiative modes are not pure electromagnetic eigenmodes of the slab, which means that they are now able to hybridize. For a laterally periodic slab, an incident wave with a specific lateral wave vector k_y can excite guided modes, because this lateral wave vector can be augmented during transmission with any reciprocal-lattice vector, bringing the final state into the radiative region. Figure 3 shows the same information as in Fig. 2, but adequate translations have been applied in order to account for the addition of reciprocal-lattice vectors to the lateral wave vector k_y (''Umklapp'' process). The applied

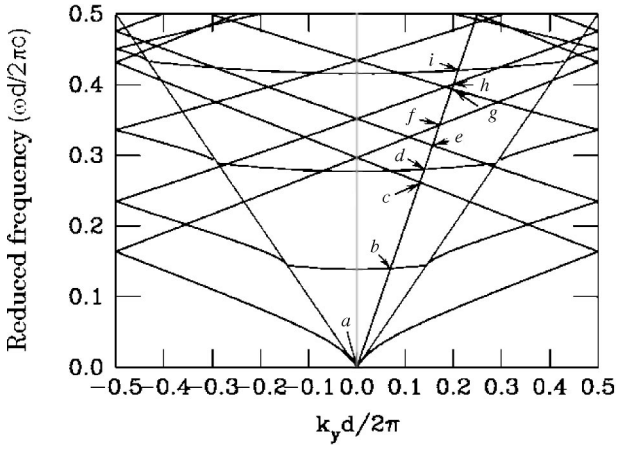

FIG. 3. The *Umklapp* process (diffraction) can bring guided modes into the radiative zone ($\omega > k_y c$) and allow their hybridization with radiative modes.

corrugation is a one-dimensional modulation of period d of the dielectric constant. The radiative zone then receives a number of new states which correspond to diffracted guided modes. Located in the region $\omega > k_y c$, these modes will be coupled to radiative modes by the periodic corrugation. For a weak periodic inhomogeneity, however, the coupling is weak and the lifetime of these guided modes is kept long.

The TE reflectance spectrum of a corrugated film, exposed to a plane wave of angular frequency ω, under an incidence $\theta = 30°$, is shown in Fig. 4. The period d of this superlattice is made of two layers of identical thicknesses, with respective dielectric constants $\varepsilon = 10$ and $\varepsilon = 13$. For an incidence angle θ, the angular frequency controls the lateral wave vector k_y by the relation

$$\omega = \frac{k_y c}{\sin \theta}, \tag{21}$$

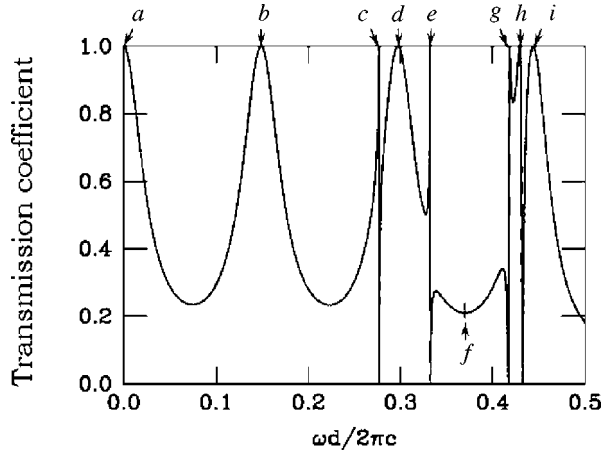

FIG. 4. Transmittance of a slightly corrugated film. The radiative modes which correspond to a transmission through the homogeneous, unperturbed film appear as a slowly varying background. The guided modes shifted back to the radiative region by the film periodicity give rise to very sharp, asymmetric structures.

here denoted as ''incidence line.'' The incidence line, above the vacuum light line, is shown in Fig. 3, where it crosses many resonant states. The crossings are labeled $a, b, \ldots, i$, and identify transmission structures on the spectrum of Fig. 4. The features a, b, d, i are related to the line crossings with the same label on the dispersion relation diagram. These broad resonances are associated with the direct transfer via radiative standing waves characteristic of a flat homogeneous film. The other features, denoted as c, e, f, g, and h arise from the guided modes, folded back by periodic diffraction, and hybridized to radiative waves because of the periodic inhomogeneity. The line shape is still very narrow; for a weak periodic perturbation, the acquired decay rate of the guided modes is kept low and the linewidth of the corresponding profiles remains narrow.

Note that these transmission mechanisms actually give rise to asymmetric transmission profiles. This asymmetrical profile finds its origin in the very different phase variations of the guided and diffused waves when sweeping the frequency. When the periodic permittivity corrugation couples the two types of waves, the transiting radiation is the interference of the guided and radiative waves with the same point (ω, k_y) in the radiative continuum. The phase of the guided wave varies very quickly around its resonance frequency, whereas the phase of the scattered wave, off-resonance, experiences nearly no phase change. One thus obtains constructive and destructive interference conditions on a very narrow frequency interval, explaining the peculiar, asymmetric transmission profile.[22]

Both types of spectral lines (Lorentzian and asymmetrical) can be exploited to create transfer functions which exhibit bistable characteristics.[23,24] As symmetric, Lorentzian characteristics, generated in Fabry-Perot structures, have already been studied for producing hysteresis cycles in transmission, we will focus the discussion here on the new possibility implied by Fano resonances in corrugated films: the use of asymmetric line shapes to produce multivalued transmission coefficients.

V. HYSTERESIS NEAR SYMMETRIC AND ASYMMETRIC SPECTRAL LINES

In this section, we use the computational scheme developed in Sec. II in order to show that asymmetric Fano resonances can lead to transmission hysteresis cycles and underline the variability of these cycles.

A. Symmetric lines

The ''standard'' (i.e., best known) hysteresis cycle appears in a planar Fabry-Perot cavity which contains a nonlinear layer. The multivalued transmission occurs when self-consistency is reached between the independent constraints that, first, the square modulus of the electric field adapts to the refractive index of the nonlinear layer (n_{nl}), as in Eq. (3), because the refractive index controls the optical path of the cavity and, consequently, the cavity tuning and the admitted field

$$n_2 |E|^2 = G(n_{nl}) \tag{22}$$

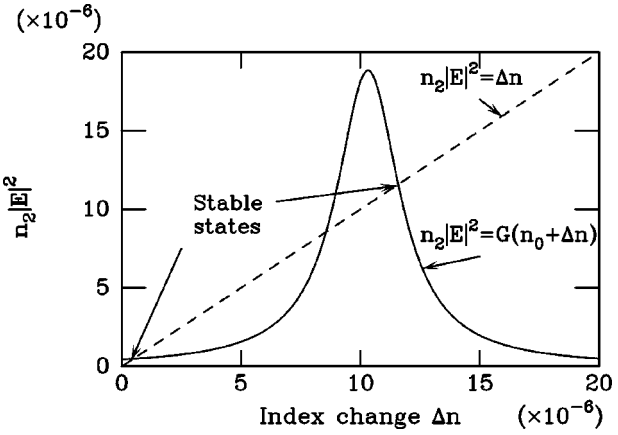

FIG. 5. Typical situation leading to a bistable transmission. A one-dimensional Fabry-Perot cavity is created in a homogeneous medium of dielectric function $\varepsilon=13$. The TE incident wave, with a wavelength of 1.5 μm, defines an incidence angle of 20° and has an amplitude such that $n_2|E_0|^2=10^{-11}$ V^2 m^{-2}. The cavity contains an homogeneous Kerr layer, 0.075 μm thick, inserted between two identical empty layers with a thickness finely adjusted to 0.380442 μm.

and, second, the square modulus of the electric field on the nonlinear layer depends on the refractive index according to the Kerr law, Eq. (1). The latter condition can also be written as

$$n_2|E|^2=n_{nl}-n_0. \tag{23}$$

For a simple, homogeneous, one-dimensional Fabry-Perot system with a thin nonlinear layer, the field and the refractive index reduce to simple scalar variables, and the solutions of this system of nonlinear equations can be viewed on a graph such as that presented in Fig. 5. On this graph, the self-consistent condition [Eq. (4)] is satisfied where the straight line meets the resonance curve, i.e., three times, two of which are stable. Changing the incident intensity means a proportional change of amplitude of the resonance curve $G(n)$. If the intensity is too weak or too large, the high-index solution disappears and the system turns back to monostable. This leads to a well-defined range of intensities where the system is bistable.

For laterally corrugated systems, the number of parameters to be obtained self-consistently is too large, and a graphic approach becomes intractable. One then has to resort to a numerical treatment. This is the case with the nonlinear Fabry-Perot system represented in Fig. 6, leading to the symmetric resonance shown in Fig. 7. Due to the inhomogeneity of the reflectors, the field inside the cavity and the refractive index on the nonlinear layer are not constant and their values at each point in the active layer must be self-consistent everywhere. The result, however (see Fig. 8), leads to characteristics very similar to those of a classical planar Fabry-Perot: at low incident intensity, the system is highly reflecting and very few light crosses the cavity. The refractive index of the nonlinear layer keeps very close to the dark value n_0, which, by positive feedback, maintains the low transmission. With increasing incident intensity, however, the

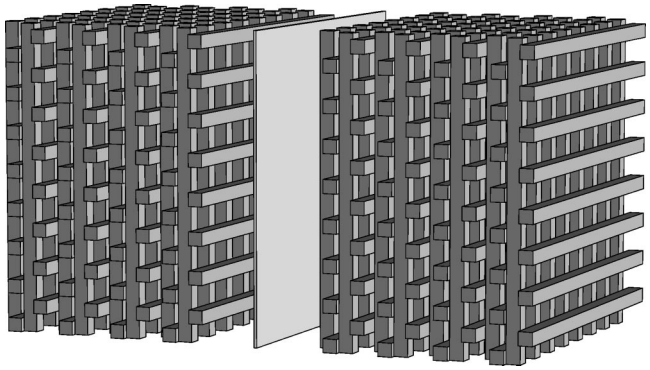

FIG. 6. Fabry-Perot cavity closed by two three-dimensional photonic-crystal films (woodpile structure of period a) acting as reflectors. Electromagnetic energy crosses this structure by optical tunnel effect, feeding the resonant cavity which contains a nonlinear layer. Each reflector film is made of four woodpile periods of total thickness $4a$, of bars with a square section $a/4$ and a dielectric constant $\varepsilon=13$. The empty cavity length is $2a$ and incorporates a central nonlinear Kerr layer of thickness $a/20$. The lateral period of these reflectors is $d=a/\sqrt{2}$.

fraction of the light transiting to the emergence side of the device starts changing the refractive index, which causes the tuning of the cavity towards a higher transmittivity. Then, an avalanche effect takes place and the system switches to a high-transmittance, high-index state. Still increasing the intensity maintains the system in this stable state. Then, for decreasing intensities, the transmission remains in this high-transparency state as long as it exists, showing a hysteresis effect. The width of the bistable intensity range depends very sensitively on the incident frequency. A memory effect is associated with the hysteresis cycle, as the system remembers its crossing of the hysteresis switching points by staying in the final transmission state. The large contrast of transmittance near the low-intensity switch point was also noticed in the case of planar devices. The transmission hysteresis loop described here will actually represent the ''classical'' hysteresis shape, to which the new shapes described in the following section will be compared.

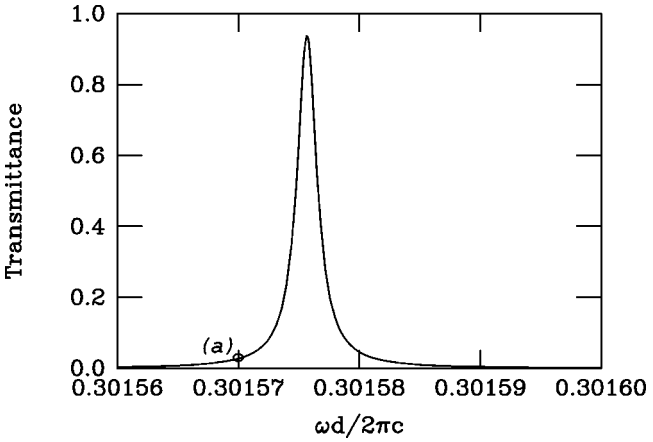

FIG. 7. Transmittance at normal incidence, showing a symmetrical resonance, for the Fabry-Perot cavity of Fig. 6. The limiting case of a dark (zero-intensity) refractive index is used.

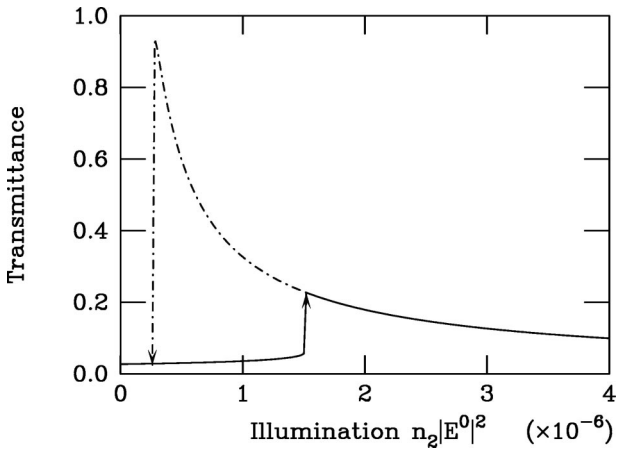

FIG. 8. Transmittance at normal incidence as a function of the incident intensity obtained for the cavity described at Fig. 6. The existence and width of a hysteresis loop very sensitively depends on the incident frequency, here chosen equal to $\omega d/2\pi c = 0.301\,570$, labeled *a* in Fig. 7.

B. Fano asymmetric lines

Figure 9 shows a totally different system. The film can be described as an homogeneous slab cut in a linear material, perforated with a triangular lattice of cylindrical holes. This geometry is designed to create well-defined Fano resonances in the transmission spectrum. The thickness of the perforated film is interrupted by a layer of nonlinear, Kerr material but

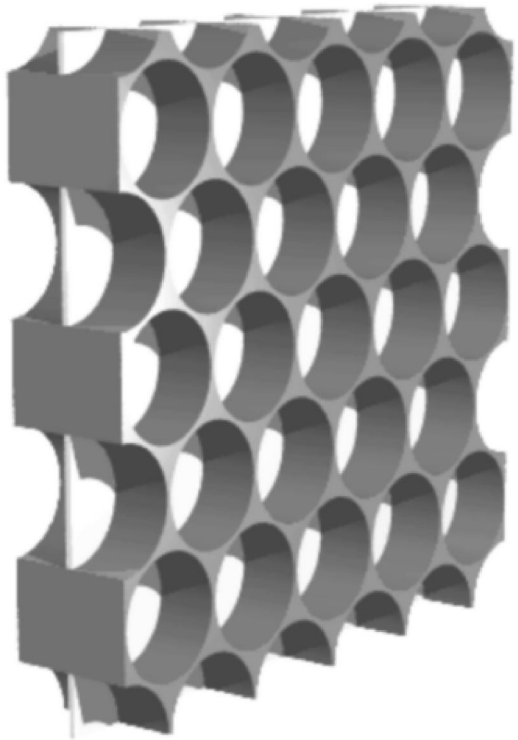

FIG. 9. Geometry of the photonic-crystal bistable film studied in this section. Reflectors are absent but a strong two-dimensional periodic corrugation of the refractive index is created along the film surfaces.

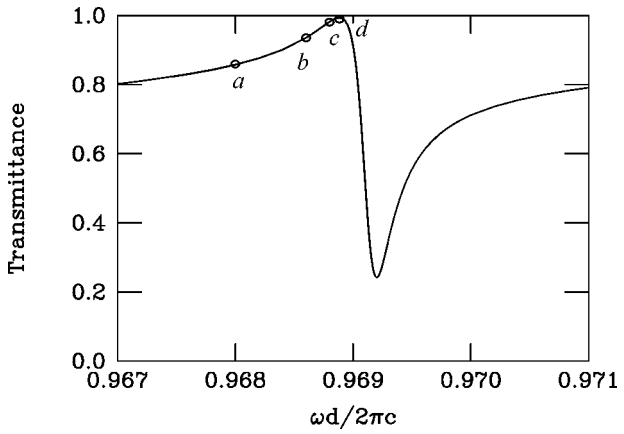

FIG. 10. Transmittance at normal incidence, in a spectral range showing an asymmetrical resonance, for the inhomogeneous film of Fig. 9. The limiting case of a dark (zero-intensity) refractive index is used.

the structure was in no way optimized for minimizing fabrication problems: our aim is here, primarily, to explore the variability of hysteresis loop shapes.

A small, detailed part of the transmission spectrum of this corrugated film is shown in Fig. 10. The linear part of the film is made from a material with a dielectric constant $\varepsilon = 13$ and the total slab thickness is represented by d. The triangular lattice of holes is such that the distance between two neighboring holes is exactly d and the radius of the holes is set to $r = 0.48d$. The nonlinear material is apparent as a layer of thickness $0.05d$ and a dark refractive index $n_0 = 2.5$ located in the cylindrical hole (this could match As_2S_3, with a nonlinear refraction coefficient $n_2 = 1.4 \times 10^{-21}\ m^2\,V^{-2}$). The line shape obtained in Fig. 10 describes a relatively abrupt change from high to low transmittance. The linewidth is still reasonably small, though the corrugation responsible for the addition of radiative components to the guided modes is particularly strong. To some extent, this can be tuned to even narrower lines by weakening the corrugation contrast: by decreasing the initial film refractive index, filling the holes with a larger index material, or reducing the hole radius.

The film transmittance as a function of the incident intensity for selected frequencies is shown in Fig. 11. The hysteresis in Fig. 11(a) spans a rather wide range of intensities which, if needed, can be reduced by narrowing the Fano line profile, as explained above. The interesting point in this hysteresis loop is that it is reversed, compared to the ''normal'' situation created by a symmetric line. The low-intensity state is highly transmitting, keeping a high and rather constant value until the system jumps into a lower transmission state. This is maintained for high incident intensities and, once the transition has taken place, for decreasing intensities. The contrast between the two transmittance states is largest at low intensity, just above the transparency threshold. The width and location of the hysteresis loop changes sensitively with the incident frequency.

At higher frequencies, closer to the dark total transmission point (see Fig. 10), the hysteresis loop encompasses a narrower intensity range [see Figs. 11(b) and 11(c)], until it

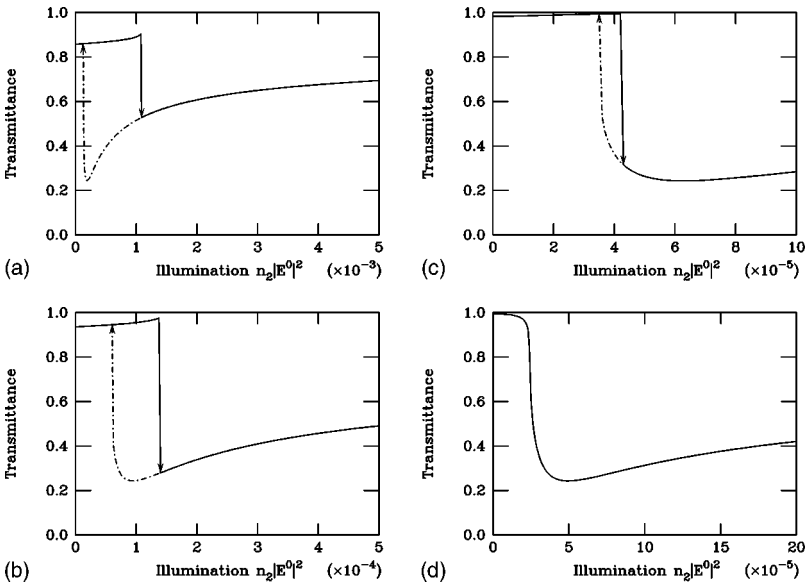

FIG. 11. Transmittance given as a function of the incident intensity, for the frequencies selected at *a*-*d* in Fig. 10. For some of these frequencies, a hysteresis cycle develops.

completely disappears [see Fig. 11(d)]. In this latter case, however, the transmission remains a sensitive function of the input intensity, fully transmitting weak signals, but cutting off much of their power above a well-defined threshold. This limitor action is already present when the hysteresis is in effect. In this case, the limitor device actually integrates a memory function; if the intensity is driven to high enough values, the system lowers its transmittance, and keeps a memory of this when brought back to lower illuminations.

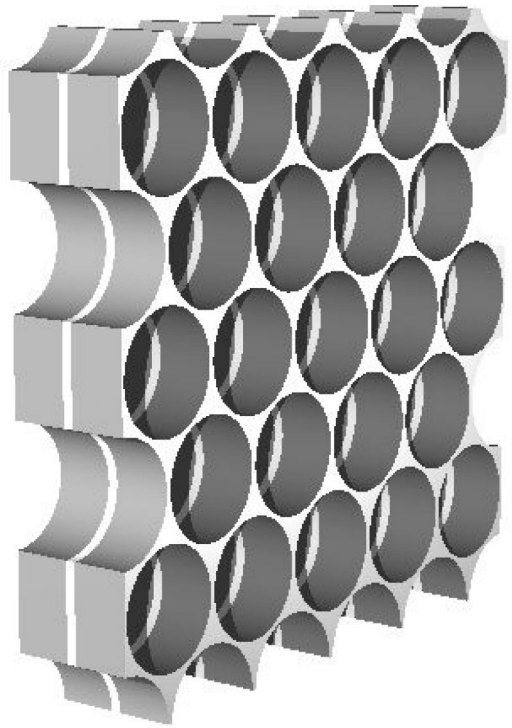

FIG. 12. Geometry of the second bistable film. In this structure, a nonlinear layer is inserted between two identical homogeneous linear films. The whole composite film is then perforated on the nodes of a triangular lattice.

The structure shown in Fig. 12 leads to a different result. Here the nonlinearity is located outside the perforations, but the geometrical parameters are the same as in the preceding example. The total film thickness is d and the dielectric constant is $\varepsilon = 13$, except in the nonlinear layer of thickness $0.05d$. The perforations again correspond to cylindrical holes with a radius $r = 0.48d$ arranged on a triangular lattice such that the distance between neighboring holes is d.

The transmission spectrum presents two ''polarizations'' of Fano resonances, which we will refer as ''descending'' or ''ascending.'' The first, descending transmission resonance (see Fig. 13) first experiences high values before suddenly dropping down to lower transparency with increasing frequencies. The second, ascending resonance (see Fig. 14) varies in the opposite way and gets depressed to a low transmission before switching to high values.

1. Hysteresis from a descending Fano resonance

A descending Fano resonance is shown in Fig. 13, as part of the transmission spectrum of the film in Fig. 12. The nonlinear behavior is quite different when the incident frequency

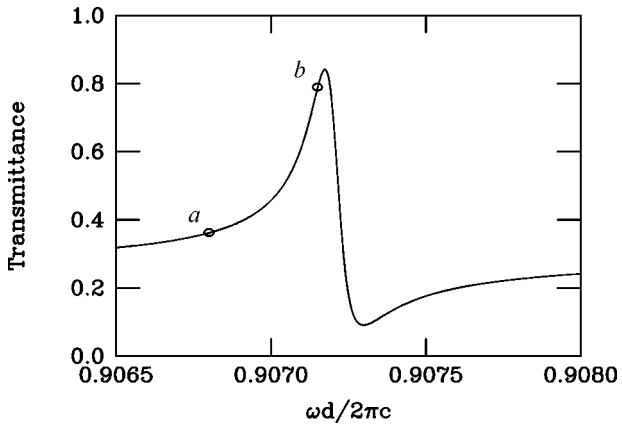

FIG. 13. Descending Fano resonance, obtained at normal incidence in the transmission spectrum of the film described in Fig. 12.

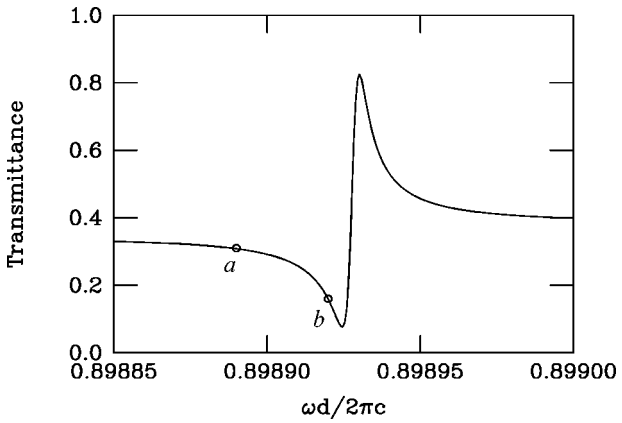

FIG. 14. Ascending Fano resonance, obtained at normal incidence in the transmission spectrum of the film described in Fig. 12.

is locked on frequencies like those indicated by *a* or *b*. A frequency in *a* is located well below the resonance, so that an increase of the nonlinear index (for increasing intensities) will lower the center of the Fano resonance, which is then driven to be swept by the incident frequency. A mechanism similar to that encountered with a symmetric resonance leads to the hysteresis loop shown in Fig. 15. This hysteresis loop is rather unusual, as it shows a crossing of the two transmission states inside the bistability range. The branch which continues the low-intensity state remains rather constant when the intensity is varied, a behavior reminiscent of that of a linear system. This ''linear'' state ceases to exist for a large threshold intensity, where the transmission switches in to a lower value. Then, coming back from the high-intensity monovalued limit, we follow a new state with a transmission depending sensitively on the incident power. This hysteresis loop actually defines a switch between a ''linear'' and a ''nonlinear'' state. The memory effect associated with the hysteresis loop allows to keep a stable record of this property. In other words, the system can be put reversibly in nonlinear response state, which will be maintained until voluntarily removed from this state.

A frequency like *b* is located near the center of the Fano resonance. Then, with increasing intensity, the change of the

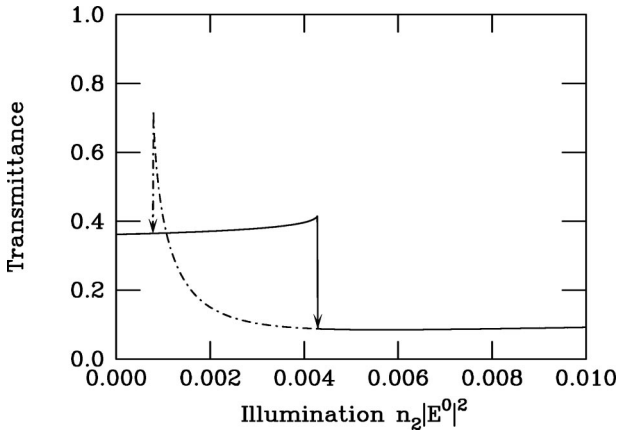

FIG. 15. Hysteresis loop for a descending Fano resonance, when the incident frequency is set off-resonance, $\omega d/2\pi c = 0.9068$, labeled *a* in Fig. 13.

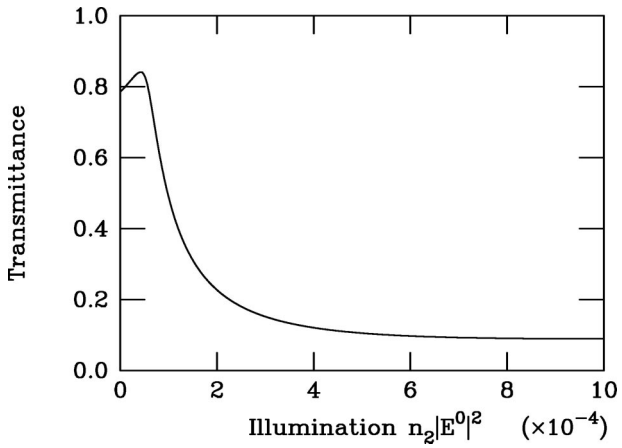

FIG. 16. Monovalued transmission for a descending Fano resonance, when the incident frequency is set close to the center of the resonance, $\omega d/2\pi c = 0.907\,15$, labeled *b* in Fig. 13.

nonlinear refractive index directly follows the incident intensity and the transmission is monovalued (see Fig. 16). The transmission coefficient decreases when the incident intensity increases, following the descending part of the spectral profile.

2. Hysteresis from an ascending Fano resonance

As shown in Fig. 14, Fano resonances can also be ascending. The transmission of the film at the frequencies denoted by *a* and *b* are shown, respectively, in Figs. 17 and 18. The frequency labeled *a* is slightly off-resonance and leads to a hysteresis cycle with a shape very similar to the one generated for a symmetric line. The frequency labeled *b* also leads to a hysteresis loop. For gradually increasing intensities, the transmission keeps constant, until the high-intensity end of the cycle is reached. Then the transmission changes abruptly to a high value. The contrast between the low and high transmission values is particularly interesting. Then, increasing again the incident intensity leads to a new constant transmission. The transmission profile in this state is a step function. Such a filter specifically starts transmission when the inci-

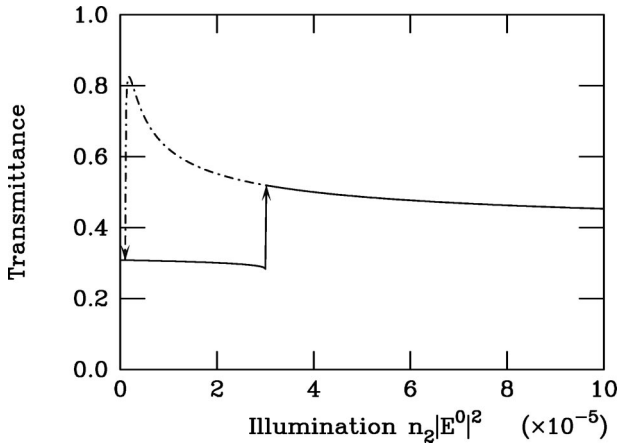

FIG. 17. Hysteresis loop for an ascending Fano resonance, when the incident frequency is set off-resonance, $\omega d/2\pi c = 0.898\,89$, labeled *a* in Fig. 14.

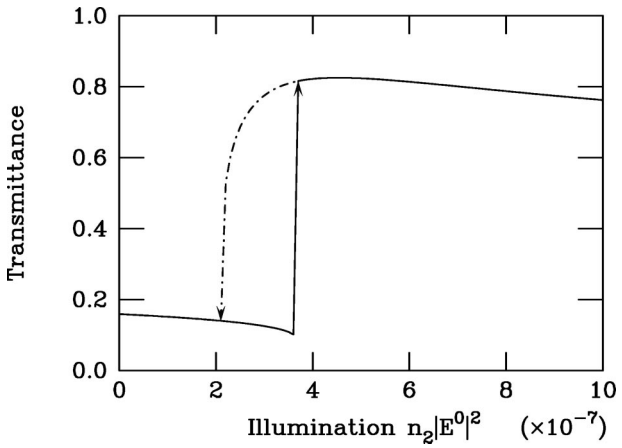

FIG. 18. Hysteresis loop for an ascending Fano resonance, when the incident frequency is set close to the center of the line, $\omega d/2\pi c = 0.898\,92$, labeled *b* in Fig. 14.

dent intensity reaches a specific well-defined value, widely adjustable by changing the incident frequency. Because of the hysteresis effect observed when decreasing the incident intensity, this transfer function is combined with a memory effect. This means that once the transition to high transparency has taken place, the system cannot jump back to the low transmission state or oscillate between the two states, even if the incident intensity fluctuates in a non-negligible manner.

VI. CONCLUSION

This paper has shown that a bistable transmission can be obtained not only with nonlinear Fabry-Perot cavities generating symmetric transmission profiles but also with corrugated photonic-crystal films generating asymmetric Fano resonances. Bistability manifests itself by the appearance of a hysteresis cycle in the diagram showing the transmission as a function of the incident intensity. The shape of the hysteresis curves associated with Fano resonances can, however, be very different from those arising from symmetric spectral lines. They are also very sensitive to the choice of the incident frequency.

In order to describe the hysteresis curves in a quantitative way, an alternative theory and alternative simulation tools were needed. The self-consistent methodology introduced in the present paper has proven particularly adequate to describe multivalued transmission coefficients in the case of monochromatic incident waves. The nonlinear problem is seen as a converging sequence of linear transmission calculations. This theory is equally applicable to planar, one-dimensional photonic-crystal films and to more complex three-dimensional structures. It is presently based on the description of the transmission coefficients by transfer matrices in a momentum-space (i.e., coupled-modes) formalism. The ideas developed in this work can easily be applied to extend other formalisms and other wave representations into the nonlinear domain.

The spectral line shape of the resonances, either symmetric or asymmetric, should be chosen narrow, so that a very weak change of the nonlinear refractive index allows for a complete scan of the line shape at the incident frequency. This puts constraints on the precision to be achieved in the geometry of the structured film and on the definition of the incident frequency. The incident wave must be very highly monochromatic, with a four-to-six figures accuracy and stability. The most difficult requirement may be the constraint on the accuracy of the geometric structure. However, these requirements can be significantly relaxed if nonlinear materials with larger values of the nonlinear refraction coefficient n_2 become available. Much research is currently conducted with this objective.

The widely adjustable shape of the hysteresis loop generated by Fano resonances may have a great impact on the design of optical signal processing devices. The transmission filters described in this paper often exhibit two processing functions simultaneously. The first one is a triggering capability, which abruptly switches the transparency towards high or low values, according to the chosen Fano profile; the second is a memory function, which tends to maintain the last visited states. This combination of functions is highly desirable for certain processing systems, like the so-called ''artificial neuron.'' This optical logical component is inherently a bipolar switch which delivers an output signal when the input intensity reaches a well-defined level. However, the output signal is only delivered to specific neighboring neurons, which are determined by a training program. The coordination of the neurons in the network has to be memorized. The combination of the trigger and memory functions, as described in this paper, can potentially be included in the design of an all-optical artificial-neuron network. This is, however, only an example. It is still difficult today to assess the exact structure of a massively parallel optical information processing system.

ACKNOWLEDGMENTS

V.L. was financially supported by the Belgian National Fund for Scientific Research (FNRS). This work was carried out with support from EU5 Centre of Excellence Grant No. ICAI-CT-2000-70029 and from the Inter-University Attraction Pole (Grant No. IUAP P5/1) on ''Quantum-size effects in nanostructured materials'' of the Belgian Office for Scientific, Technical, and Cultural Affairs. We acknowledge the use of Namur Interuniversity Scientific Computing Facility (Namur-ISCF), a common project between the Belgian National Fund for Scientific Research (FNRS), and the Facultés Universitaires Notre-Dame de la Paix (FUNDP).

*Electronic address: virginie.lousse@stanford.edu

[1] S.D. Smith, Appl. Opt. **25**, 1550 (1986).
[2] H.M. Gibbs, S.L. McCall, and T.N.C. Venkatesan, Phys. Rev. Lett. **36**, 1135 (1976).
[3] F.S. Felber and J.H. Marburger, Appl. Phys. Lett. **28**, 731 (1976).
[4] J.H. Marburger and F.S. Felber, Phys. Rev. A **17**, 335 (1978).
[5] Qiming Li, C.T. Chan, K.M. Ho, and C.M. Soukoulis, Phys. Rev. B **53**, 15 577 (1996).

[6] C. Manolatou, S.G. Johnson, S. Fan, P.R. Villeneuve, H.A. Haus, and J.D. Joannopoulos, J. Lightwave Technol. **LT-17**, 1682 (1999).
[7] S. Radic, N. George, and G.P. Agrawal, J. Opt. Soc. Am. B **12**, 671 (1995).
[8] H.M. Gibbs, *Optical Bistability: Controlling Light with Light* (Academic Press, New York, 1985).
[9] H.M. Gibbs, S.L. McCall, and T.N.C. Venkatesan, Phys. Rev. Lett. **36**, 1135 (1976).
[10] T.N.C. Venkatesan and S.L. McCall, Appl. Phys. Lett. **30**, 282 (1977).
[11] H.M. Gibbs, and S.L. McCall, T.N.C. Venkatesan, A.C. Gossard, A. Passner, and W. Wiegmann, Appl. Phys. Lett. **35**, 451 (1979).
[12] S.L. McCall, Appl. Phys. Lett. **32**, 284 (1978).
[13] H.M. Gibbs, S.L. McCall, A. Passner, A.C. Gossard, W. Wiegmann, and T.N.C. Venkatesan, IEEE J. Quantum Electron. **QE-15**, 108D (1979).
[14] A. Migus, A. Antonetti, D. Hulin, A. Mysyrowicz, H. Gibbs, N. Peyghambarian, and J. Jewell, Appl. Phys. Lett. **46**, 70 (1985).
[15] P.W. Smith, E.H. Turner, and P.J. Maloney, IEEE J. Quantum Electron. **QE-14**, 207 (1978).
[16] U. Fano, Phys. Rev. **124**, 1866 (1961).
[17] S. Fan and J.D. Joannopoulos, Phys. Rev. B **65**, 235112 (2002).
[18] A. Calderone and J.P. Vigneron, Int. J. Quantum Chem. **70**, 763 (1998).
[19] V. Lousse and J.P. Vigneron, Phys. Rev. E **63**, 027602 (2001).
[20] W. Kohn and L.J. Sham, Phys. Rev. **140**, A1133 (1965).
[21] J.B. Pendry and A. MacKinnon, Phys. Rev. Lett. **69**, 2772 (1992).
[22] S. Fan, W. Suh, and J.D. Joannopoulos, J. Opt. Soc. Am. A **20**, 569 (2003).
[23] M.G. Banaee, A.R. Cowan, and Jeff F. Young, J. Opt. Soc. Am. B **19**, 2224 (2002).
[24] A.R. Cowan and Jeff F. Young, Phys. Rev. E **68**, 046606 (2003).